Relative role of short interfacial fingers and long internally driven streamers in convective flows below growing sea ice

C. A. Middleton [1,2,3] S. S. Gopalakrishnan [1,4] I. Berenstein [1] B. Knaepen [4]
J.-L. Tison [2] and A. De Wit [1]

[1]*Université libre de Bruxelles (ULB), Nonlinear Physical Chemistry Unit, CP231, 1050 Brussels, Belgium*
[2]*Université libre de Bruxelles (ULB), Laboratoire de glaciologie, 1050 Brussels, Belgium*
[3]*School of Engineering, University of Liverpool, The Quadrangle, Brownlow Hill, Liverpool, L69 3GH, United Kingdom*
[4]*Université libre de Bruxelles (ULB), Service de physique statistique et plasmas, CP231, 1050 Brussels, Belgium*

Convective dynamics developing below growing sea ice are studied experimentally by freezing salt water from above in a quasi-two-dimensional Hele-Shaw cell. Observations of the convective processes are made with Schlieren and direct imaging systems, allowing visualization both under and within the growing ice. Buoyancy-driven flows are seen to develop under the ice layer via two different mechanisms: On one hand, brine diffuses out from the ice layer creating a denser boundary layer of enhanced salinity, which triggers boundary layer convection resulting in small-scale interfacial fingers. On the other hand, internal flow within brine drainage channels inside the ice is observed flushing out longer-scale convective streamers at given locations at the ice-water interface. Streamers descend in the bulk aqueous layer faster and for longer distances than fingers. Simulations confirm that, despite nonlinear interactions between fingers and streamers, the different speeds observed can be correlated to different density differences between the interfacial or internal rejection and the underlying bulk salt water. Estimates of relative mass fluxes through the interface by the two mechanisms suggest that, when streamers are active, the mass of salt rejected through the streamer pathway can be larger than the one expelled through the finger pathway. However, as fingers are maintained throughout the ice growth while the rejection from brine channels features an intermittent "on-off" behavior, there are certain periods of time when the mass flux of the two mechanisms is similar, but also some time intervals during which the flux due to interfacial short fingers becomes dominant.

I. INTRODUCTION

As sea ice grows from sea water, the salt initially dissolved in the liquid phase is rejected from the solid phase. This salt concentrates into areas of liquid brine, such that sea ice is often described as a mushy layer, where the solid phase is bathed in the concentrated brine [1–3]. However, it is known that sea ice becomes less saline over time [4,5]. There is current interest in understanding the transport processes at the origin of this expulsion of brine out of the growing sea ice due to their impact on global climate processes. Highly saline brine sinking from sea ice is a driver of global thermohaline circulation [6–9], while convective movements of brine also influence the movement of gases and nutrients, which affect the polar ecosystems [10,11]. Recent experimental work has shown that convection diagnosed by explicitly using a Rayleigh number approach performed well (as compared to diffusion or a simpler convective parametrization) to resolve salinity profiles and the distribution of other dissolved tracers, decoupled from salinity [12].

Several transport mechanisms contributing to this desalation have been observed at different stages during ice growth and decay [4,13–15]. The dominant mechanism during ice growth is thought to be internal buoyancy-driven convection through channel structures driven by density differences between the brine in the ice layer and the underlying salt water [13,15]. This convection results in the "chimneys" or the "mushy-layer mode" of the mushy layer literature [1–3]. It becomes possible when critical values of permeability, temperature, and brine volume fraction are reached in the ice [12,16]. Salt segregation below the ice-water interface (interfacial convection) has also been suggested as a brine rejection mechanism during ice growth [4,5,15]. This triggers interfacial fingers corresponding to the "boundary-layer mode" of the mushy layer theory [1–3]. A stability analysis that identifies the origins of these modes has been developed by Worster [17]. Prior experimental and field observations have suggested that this interfacial mechanism only produces a negligible amount of brine movement [15,18]. However, our earlier experimental work has suggested that interfacial convection may be more important than previously thought [19,20].

In order to study these different desalination mechanisms in the laboratory, it is possible to exploit the fact that liquids of different densities have different refractive index properties using optical techniques such as shadowgraphy and Schlieren methods. Wettlaufer *et al.* used shadowgraphy to visualize high-density brine sinking from a growing sea ice layer into the underlying less dense sea water in a three-dimensional (3D) tank [18]. Two different mechanisms of brine rejection were observed: initial weaker rejections, interpreted as interfacial convection, and later stronger rejections, interpreted as due to internally driven convection, thought to replace the initial interfacial convection. Wakatsuchi and Ono used Schlieren optical methods to visualize rejections from sea ice in a 3D tank, allowing a dependence of the dynamics on the growth rate of the ice to be found [21]. In our previous work, we have also applied this Schlieren method to visualization of rejections from a growing ice layer, within a quasi-two-dimensional (2D) Hele-Shaw cell [19,20]. Our results showed that interfacial and internal convection (referred to as fingers and streamers, respectively, throughout the current article) may be concurrent throughout ice growth.

The objective of the current work is to quantify experimentally the relative importance of interfacial and internal convection during initial ice growth and analyze their relative contribution in mass fluxes from the ice towards the water below it. We achieve this via experiments freezing a NaCl salt solution from above in a dedicated quasi-2D Hele-Shaw cell. We visualize subsequent ice growth and brine rejection in the water with a Schlieren visualization system [19,20], along with an additional superimposed direct imaging system which allows visualization of brine channels within the ice layer. We develop an image analysis technique that allows us to study the convective dynamics both below and within the ice and quantify the properties of both interfacial small fingers and longer-scale streamers. We find that streamers descend faster than fingers into the underlying water layer and feature an on-off behavior, whereas fingers appear to be generated continuously. Complementary simulations of the problem describing buoyancy-driven convection in the lower host phase compare the speed of descent of the interacting streamers and fingers as a function of their relative densities. On the basis of the number of fingers and streamers active over time as well as their relative densities, we compare the predicted ratio of salt mass rejected through the streamers and fingers. We find that the mass flux is higher in streamers than in fingers when the former are active. However, the fact that the salt rejection from streamers is sometimes interrupted while the rejection through fingers is continuous in time suggests that interfacial convection might have a more important contribution to brine transport from the ice towards the water than previously thought.

II. EXPERIMENTAL METHODOLOGY

Experimental runs were carried out in a custom-designed Hele-Shaw cell, previously described in [19]. This cell consists of two Plexiglas plates (of thickness 10 mm) oriented vertically, with internal cell dimensions of 64 cm × 34 cm × 3 mm [Fig. 1(a)]. The cell was mounted within a Z-type Schlieren optical system, which visualizes gradients of refractive index highlighting the
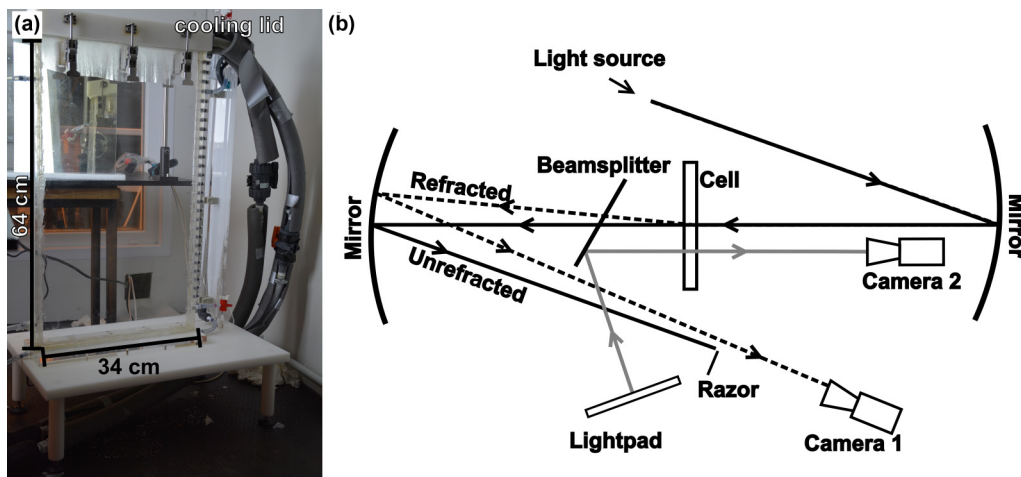
FIG. 1. Experimental setup. (a) Vertical Hele-Shaw cell cooled from above with a cooling lid fed by alcohol pipes, with ice growing from the lid downwards. (b) Schematic of the superposed imaging systems. The light paths generated in the Schlieren imaging system are shown in black, with solid and dashed lines showing unrefracted and refracted light paths, respectively. The direct imaging light paths are shown in gray.

position of higher salinity brine rejections within the lower salinity bulk reservoir [19,20,22]. The area of the Hele-Shaw cell which can be visualized is dependent on the size of the parabolic mirrors (here 20 cm in diameter). The camera image was therefore focused on the center of the illuminated circle to monitor the largest depth possible into the cell, resulting in Schlieren images of 9 cm width and 14 cm depth.

Superimposed on the Schlieren imaging device was a direct imaging system illuminating the ice from behind with a lightpad. This superposition is achieved with a beamsplitter, which allowed 50% of the incident light of the lightpad to pass through the cell and reflected the other 50%. The beamsplitter was positioned such that the light paths from the two optical systems did not interfere with each other [Fig. 1(b)]. Direct imaging allows details of the structures within the ice layer to be visualized at the same time as the underlying convective dynamics are captured with the Schlieren system. The cell and imaging systems were placed in an environmental chamber maintained at a temperature of $0\,°C$. An additional cooling temperature is applied along the top of the cell, by flowing alcohol at a temperature of $-20\,°C$ through a specially designed lid [Fig. 1(a)]. The whole setup is mounted in a cooled chamber.

Several hours before an experimental run, the Hele-Shaw cell was filled with an NaCl salt solution of 35 ppt (35 g NaCl per kg of solution, chosen to represent an average sea water concentration), and the whole apparatus allowed to equilibrate to the $0\,°C$ temperature of the environmental chamber. One camera was positioned to take images of the area of the cell illuminated by the Schlieren system, and another one to take direct images of the ice layer. To begin an experimental run, cooling from above was initiated. As the forcing temperature of $-20\,°C$ is below the freezing point of salt water at this concentration, a downward moving freezing front was produced, generating a layer of growing sea ice above a layer of liquid salt solution. Time lapse images were taken with both optical systems every 10 sec, allowing tracking of the dynamic convective processes. Further details of the apparatus can be found in [19,20]. Three repeat experiments were carried out. Images were collected for approximately 22 h for each experiment.

III. FINGERS AND STREAMERS

Over time, the ice layer increases in thickness, as can be seen in the series of images shown in Fig. 2 and in the movie available as Supplemental Material [23].
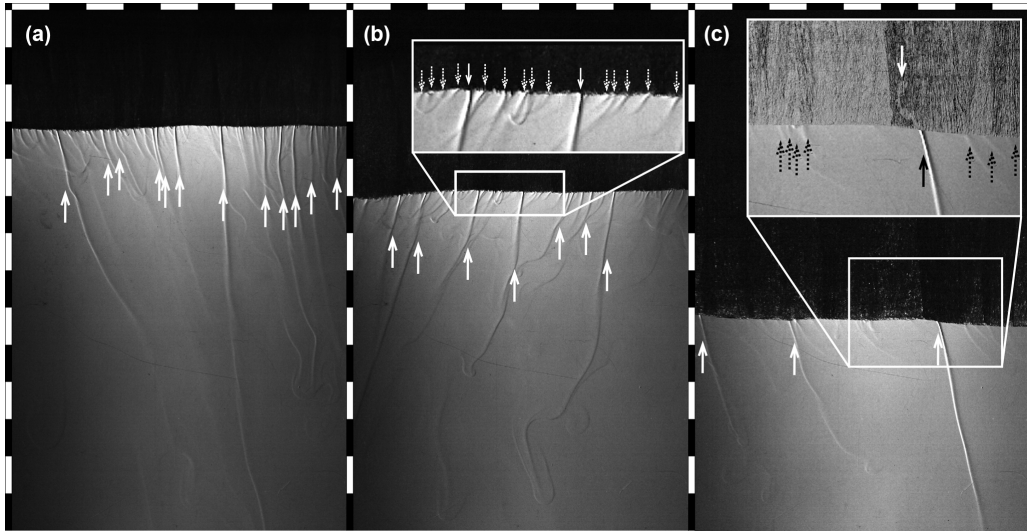
FIG. 2. Schlieren images of the convective dynamics for an ice thickness of (a) 30 mm, (b) 50 mm, and (c) 80 mm when a 35 ppt NaCl solution is cooled at $-20\,°C$ from above in a chamber kept at $0\,°C$. The dark region at the top is the ice layer, and the gray area is the underlying water. Long streamer positions are marked with solid arrows while the zoom insets in (b) and (c) also indicate short finger positions with dashed arrows. The inset in (c) is a composite figure, where the direct imaging view of the ice layer is superimposed on the Schlieren image, allowing the streamer in the water to be linked to a channel structure in the ice layer, indicated by the solid white arrow. Alternate black and white border scales are in cm.

For all three experimental runs, as the freezing front progresses, the ice thickness increases in a reproducible manner (Fig. 3). The Schlieren images show the ice as a black layer but give information on convective processes within the bulk solution below the ice. In particular, the Schlieren view identifies two different populations of brine rejections: from early on and throughout
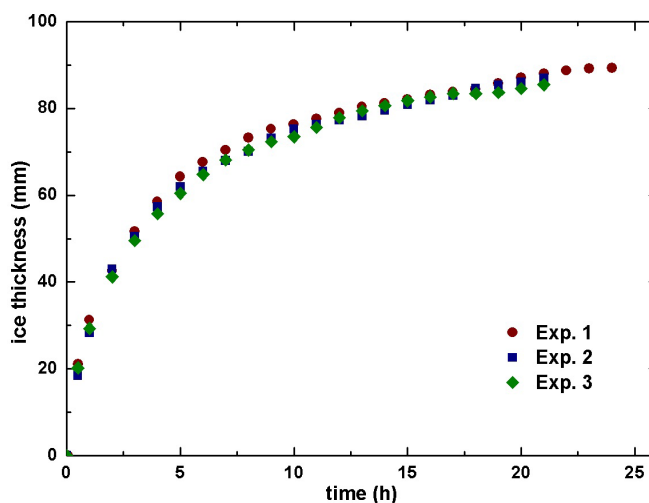

FIG. 3. Ice thickness as a function of time for three different experiments following ice growth of a 35 ppt NaCl solution in a Hele-Shaw cell with the upper lid cooled at a $-20\,°C$ within an environmental chamber temperature of $0\,°C$.

the ice growth, short-scale, lower definition fingers (marked with dashed arrows in the inset figures) are seen to sink just below the interface up to 3–4 cm maximum in depth in the aqueous layer. These fingers cannot be correlated to any motion within the ice [inset in Fig. 2(c)] and are thought to be due to salt rejection just below the ice-water interface. After about 10 min, additional long, well-defined streamers (marked with solid arrows on Fig. 2) start to sink in the bulk salt solution. These streamers can be seen to originate from channel structures in the ice layer, seen when the direct image of the ice layer is superimposed on the Schlieren image [inset in Fig. 2(c)], and extend much longer distances in the bulk.

These channels in the ice are more easily seen in the video in the Supplemental Material [23]. The streamers also feature back and forth lateral movements due to the fact that the channel they originate from in the ice meanders in time as the ice layer grows. Sometimes, merging between two streamers or between a finger and a streamer is observed. While the fingers remain present throughout the experiment, the situation is more variable for streamers. Indeed, sometimes one streamer shuts down when the brine channel it originates from freezes again. This results in an "on-off" intermittent regime for streamers with their number and spatial location varying in time. A more detailed image analysis allows us to quantify the relative role of fingers and streamers in the dynamics.

IV. IMAGE ANALYSIS

In order to quantify the convective dynamics, Schlieren images are first divided by a reference initial image taken before cooling begins. This processing highlights the changes occurring due to ice growth and brine rejection and removes experimental artifacts.

A. Space-time dynamics

Space-time plots are generated from these divided images by binarizing each image such that the ice layer is black and the underlying water (including the streamers and fingers) is white. For each column of pixels along the width, the ice interface can then be located as the point where this transition between black and white areas occurs. Once the ice interface is located, a separate binarization using a lower threshold allows fingers and streamers to be more clearly identified than in the grayscale images. A single row of pixels at both 1 and 3 cm below the location of the interface are then copied as a function of time to generate space-time plots of the dynamics (Fig. 4). Each image is analyzed in sequence, and, as the interface progresses downwards, the sampled position copied to the space-time plot also moves down in the cell.

The space-time plots sampled 1 cm below the ice interface show more activity than those sampled 3 cm below (Fig. 4) due to the presence just below the ice of the small interfacial fingers with a limited vertical extent. The two populations of rejections can indeed be distinguished by their relative intensities and their different penetration depths. Streamers are seen as darker traces in the space-time plots, at both 1 and 3 cm below the interface. The onset of streamer activity is not immediate. As seen in Fig. 4(a), streamers appear only after a while, whereas fingers develop earlier. Nevertheless, once streamers are established, they often persist in the same position throughout the time period shown, with small lateral oscillations around that fixed position. However, the number of streamers does not remain constant throughout time: certain streamers become active during the time shown and others stop and then restart again in an "on-off" behavior (see examples marked with ovals in Fig. 4). The three lines in Fig. 4(d) highlight the variation in the number of streamers over this time period. Lines 1, 2, and 3 transect 0, 4, and 6 streamers, respectively. When active, streamers at 1 cm below the interface show a slight oscillation about an otherwise constant position, this movement becomes more apparent further from the interface. Merging of streamers is present, as indicated with rectangles in Figs. 4(a) and 4(d). Fingers can be seen to drift towards the longer streamers in certain places [e.g., rectangles in Fig. 4(b)]. The number of fingers and streamers observed over the first 15 h of the three experiments is shown in Fig. 5(a). There are significantly
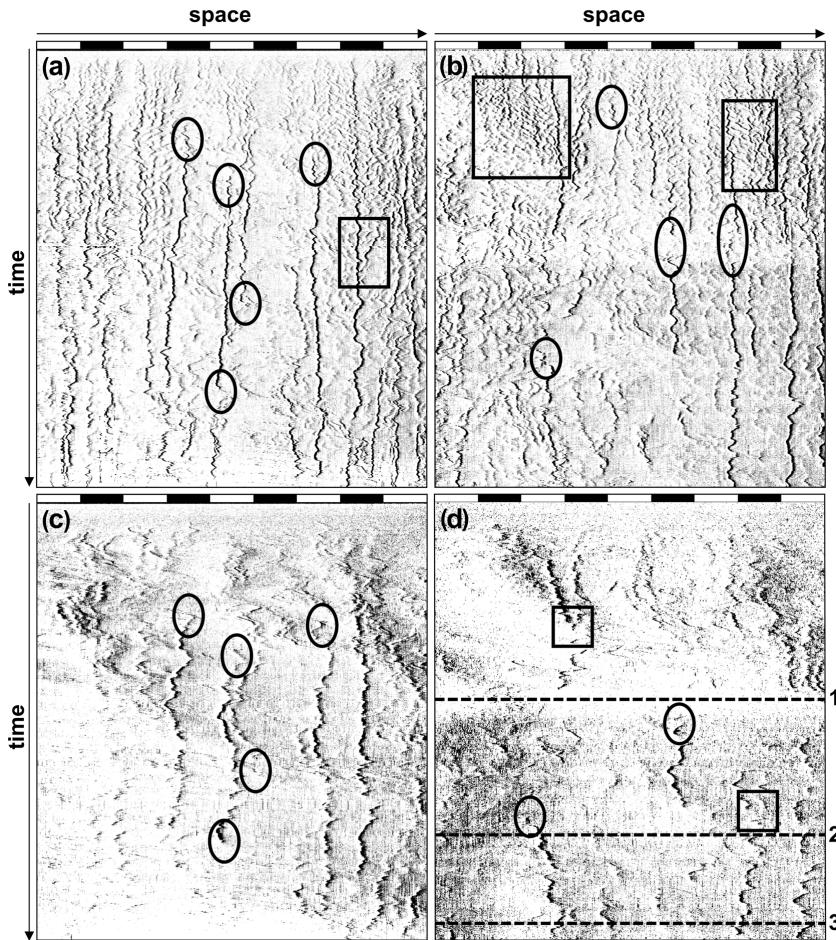
FIG. 4. Space-time plots showing the streamers and fingers dynamics along a horizontal line under the ice interface during the first 150 min of experiments (time pointing downwards). Alternate black and white border scales are in cm. (a) experiment 2: 1 cm below the ice interface; (b) experiment 3: 1 cm below the ice interface; (c) experiment 2: 3 cm below the ice interface: (d) experiment 3: 3 cm below the ice interface. Original images have been divided by a reference image. Ovals indicate stopping or starting incidences of streamers. Rectangles indicate merging of streamers in (a) and (d) and fingers merging with streamers in (b). The three lines in Fig. 4(d) highlight the variation in the number of streamers over time.

larger amounts of fingers than streamers at all times, and both streamers and fingers decrease over this time period. Indeed the number of streamers is limited to seven or eight when they start to appear while only two to four survive after 10 h. Similarly, while 30–40 small fingers are observed below the interface at the beginning of the ice growth, only 17–25 remain at the end of the recording.

The number of streamers present at a given time are fairly easy to identify from the Schlieren images as the gradient across a rejection is well defined (e.g., Fig. 2). The streamers are also associated with channel structures which can often be identified in the ice layer in the direct imaging figures. However, due to the small number of brine channels present in the necessarily restricted experimental cell, differences between experiments may be magnified i.e., stoppage of one brine streamer could represent a fairly high percentage of the brine channels visualized.

The number of fingers is less simple to identify, as there is no structure within the ice layer to support any rejection definition, so this relies entirely on the refractive index effect in the Schlieren image. One advantage for identification of fingers is that they are shorter than streamers, so a new
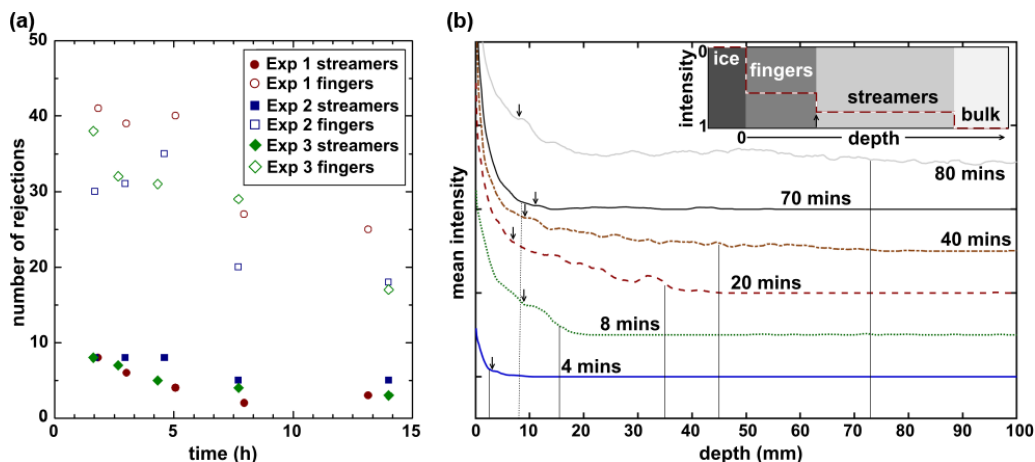
FIG. 5. (a) Temporal evolution of the number of streamers (solid symbols) and fingers (open symbols) for the three experiments. There is a larger number of fingers than streamers, and the number of both streamers and fingers decrease over the course of time. (b) Averaged image intensity profiles for experiment 3 against the depth below the ice-water interface at given times. The inset shows an idealized profile in the situation where boundaries between layers are distinct. Profiles are staggered along the y axis to allow details to be observed. Vertical lines indicate approximate mixing length (L_s) for each time. Arrows indicate inflections used to calculate length of fingers (L_f). Note the decreased mixing length at 70 min (dashed vertical line) when compared to both 40 min and 80 min. Bumps in the profiles, such as at 20 min at approximately 30 mm, are a signature of the convective processes in the bulk water.

tip of the rejection appears more often and is more easily identified than the streamers, particularly in videos (e.g., Supplemental Material [23]).

The relatively large range of values for rejections between the three experiments shown here are likely due to a combination of the restricted experimental setup, and smaller field of view, magnifying small fluctuations in the experimental behavior. Yet the trend that fingers systematically outnumber the streamers as seen in Fig. 5(a) is robust.

B. Transverse averaged profiles and mixing lengths

To obtain insight into the average extension of the convective zone, we compute transverse averaged intensity profiles. To do so, the normalized images of the dynamics are binarized with a given threshold, such that white pixels correspond to no change from the reference image (the undisturbed liquid layer) while black pixels correspond to a change from the reference image (indicating the presence of ice, fingers, or streamers). We next average the black and white pixels across the width of the image to obtain an average intensity of the binarized image as a function of the depth in the aqueous solution [see Fig. 5(b)]. A value of this average intensity equal to 0 indicates the presence of ice, values between 0 and 1 indicate fingers and streamers, and values of 1 indicate the undisturbed liquid layer. The inset sketch in Fig. 5(b) shows an ideal situation, where interfaces between layers are all clearly defined. This situation would occur if rejections were all consistent lengths and widths and did not interact with the surroundings. Unfortunately, this is not the case, as can be seen in Fig. 2; therefore, interpretation of the profiles, and location of the boundaries between layers, is necessarily somewhat subjective.

The total mixing length of rejections is calculated using the ice interface position and the total depth of penetration of brine rejections. As an undisturbed liquid layer is indicated by a value of 1 in the intensity profile, the depth at which this is found in the intensity profile is the total depth of penetration of brine. In order to remove problems associated with noise in the processed image,
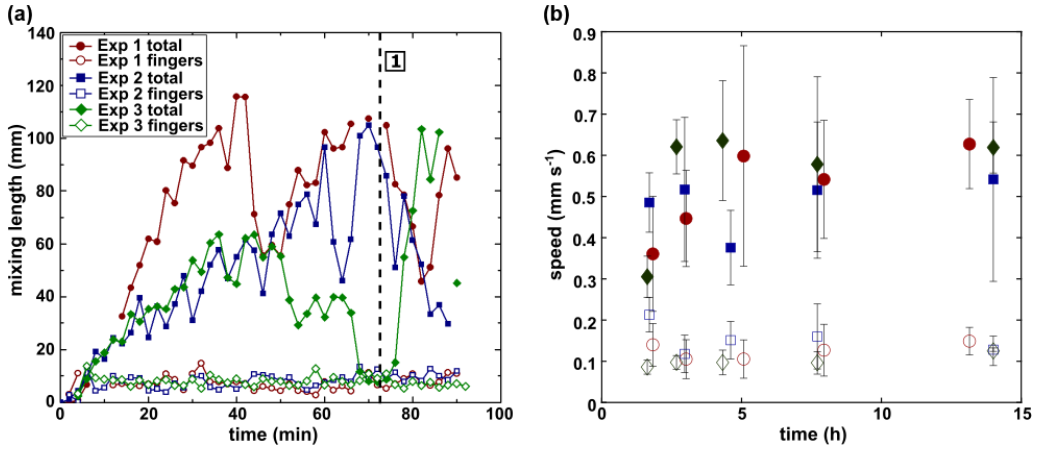
FIG. 6. (a) Temporal evolution of the mixing lengths in three experiments with the same cooling from above and the same salinity. Solid and open symbols represent the total mixing length following the most downward tip of streamers and fingers, respectively. The dashed black line shows a large drop in total mixing length in experiment 3 and corresponds to line 1 in Fig. 4(d), where all streamers have become inactive. (b) Average downward vertical speed of streamers (full symbols) and fingers (open symbols) as a function of time. Each data point represents an average of the speed of three individual rejections with its standard deviation.

the threshold for the position of the end of brine rejections was not set exactly at 1, but rather 0.98. This threshold may result in underestimations of the mixing length, but as the threshold was kept constant between experiments, relative comparisons between experiments are still valid.

Two mixing lengths were then defined due to either internal generated streamers (L_s) or interfacial finger (L_f) convection, as the distance between the ice-water interface and the end of the visualized disturbance in the liquid layer caused by each rejection mechanism [Fig. 6(a)]. In early profiles, where only fingers are present (i.e., before streamer development) the finger length is equal to the total mixing length. When both fingers and streamers are present, the mixing length reported is inevitably that of the streamers (L_s). Determination of the mixing length L_f of the fingers, when streamers are present, is therefore more complicated and requires subjective analysis of the detail of the intensity profile, combined with information from the original images.

Earlier in ice growth, the intensity reaches a plateau indicating undisturbed bulk water at a depth very close to the ice interface. Over time, the profiles show more variability, with an initial sharper change, then a more gradual change, with some variability. A particularly interesting profile is that at 70 min, which shows more resemblance to profiles at 4 and 8 min (i.e., no bumps) than that of 40 or 80 min, with a sharp initial change in intensity.

By examining the detail of the intensity profile at 4 min, it can be seen that an inflection in the profile exists, where the gradient changes as the intensity moves towards a constant value. This inflection is taken to be the end of the interfacial convective layer, equivalent to the "step" between fingers and streamers in the idealized scenario in the inset. Similar inflections exist in the other profiles, although these are less marked, due to the complicating presence of streamers. After visual inspection of the original images, these inflections are considered to represent the depth of the fingered zone (i.e., the length L_f of the fingers).

Figure 6(a) shows the temporal evolution of the finger and streamer mixing lengths. It can be seen that the length of small fingers is fairly constant in time with little variation between the three experiments. In contrast, the total mixing length is much more variable, with larger differences in time and between the three experimental runs. An initial increase in mixing length is followed by a period of episodic decreases and increases. For experiment 3, the mixing length L_s drops significantly at a time of 50 min and then decreases further at 70 min to the same value as the length

of the fingers (dashed black line). This drop corresponds to the 70 min intensity profile in Fig. 5(b), and Line 1 in the space-time plot in Fig. 4(d), where it can be seen that there are no active streamers at that moment. It can also be seen in the video in the Supplemental Material [23], where all of the streamers that were present after half an hour, shut off at 70 min leaving only fingers present. A similar (though less drastic) strong drop occurs in experiment 1 after 45 min and in experiment 2 roughly around 65 min.

C. Speed of fingers and streamers

One limitation of the Schlieren method, as applied here, is the inability to measure steady-state velocities of the observed fingers and streamers. Only the speed at onset of streamers or fingers descent can be measured, where a density difference is visible at the tip of the rejection. Alternative methods such as particle image velocimetry (PIV) would allow steady-state measurements, but the inclusion of particles would affect the dynamics within the growing ice. The temporal evolution of the tip position of individual starting streamers and fingers allows determination of their descent speed into the underlying bulk salt water. The necessity for a streamer tip to be visible also decreases the amount of measurements possible. For a given ice thickness, three streamers which restarted were followed and their tip tracked to calculate the speed of descent. As these events do not happen continuously, it was necessary to consider a range around the desired thickness to find three streamers to measure. In parallel, measurable fingers were easier to locate as new generations of fingers were continuously replenished. The descent speeds of three fingers were therefore measured at the same time as each streamer. The average of each set of measurements for fingers and streamers is shown in Fig. 6(b). The maximum vertical speed U measured is of the order of 0.7 mm/s. The kinematic viscosity ν of water is 1 mm^2/s. Taking the gap width $H = 3$ mm of the Hele-Shaw cell as a characteristic length, we compute a Reynolds number Re $= UH/\nu = 2.1$. As this number is low, the flow in the liquid layer is not in a turbulent regime. We measure the speed of the fingers and streamers just as they come out of the ice, so we assume it is not affected by the nature of the convective flow in the bulk. We can see that the speed of streamers is higher than that of the fingers by a factor 2–3, and that the finger speed is more constant than that of the streamers. There is a slight upward trend in streamer speed with time likely due to a combined effect of increased brine density (colder temperatures) and increased brine fluxes (larger catchment area) over time.

V. NUMERICAL SIMULATIONS

In homogeneous cases, the speed of descent of one liquid within another miscible one is necessarily a linear function of the relative densities between the two solutions [24]. The different speeds achieved by streamers and fingers at the same time into the same bulk salt solution suggest, therefore, that their brine content is different but in each case larger than in the bulk solution. As they propagate, the fingers and streamers affect each other through nonlinear interactions. In particular, merging between fingers and streamers like seen in Fig. 4(b) might locally change the density and thus the descent speed. It is thus not obvious that the behavior of independent fingers in homogeneous systems holds here, and we perform numerical simulations to confirm whether such interactions result in descent speeds still proportional to their intrinsic densities at the interface between the ice and the fluid domain.

To compare these speeds and obtain quantitative information useful in the evaluation of mass fluxes, we perform nonlinear simulations of the dissolution from above of a solute A within a 2D aqueous layer. Contrary to other simulations that incorporate the internal convective dynamics inside the ice layer [3,25–27], we focus here only on the water layer within the Hele-Shaw cell, similarly to studies of convective dissolution [28–30]. The buoyancy-driven flow evolution in a thin enough quasi-2D Hele-Shaw cell is described, as for flows in porous media, by Darcy's equations [24] coupled to the advection-diffusion equation for the concentration A of the salt via a state equation for density. Assuming a linear increase of density with the salt concentration, the equations read in

dimensionless form as [31]

$$\nabla p = -\mathbf{u} + A\hat{\mathbf{y}},$$
$$\nabla \cdot \mathbf{u} = 0, \tag{1}$$
$$\partial_t A + \mathbf{u} \cdot \nabla A = \nabla^2 A,$$

where p is the pressure, $\mathbf{u}$ is the velocity, and $\hat{\mathbf{y}}$ is the unit vector pointing downwards in the direction of gravity. The equations are nondimensionalized using the initial concentration A_F of salt rejected in the finger by dissolution, the characteristic speed $\mathcal{U}$, which is related to the strength of buoyancy forces, namely, $\mathcal{U} = gK\alpha A_F/\mu$, the characteristic length $\mathcal{L}$ given by the balance of diffusion and advection $\mathcal{L} = D\phi/\mathcal{U}$, and the characteristic time $\mathcal{T} = \mathcal{L}/\mathcal{U}$, where g is the magnitude of the acceleration due to gravity, $K = a^2/12$ is the permeability, a is the gap width of the cell, α is the solutal expansion coefficient of species A, D its diffusion coefficient, μ is the dynamic viscosity, and ϕ the porosity, taken here as 1. The initial conditions are given by

$$A = A_S/A_F, \quad \mathbf{u} = \mathbf{0} \quad \text{for} \quad y = 0, \quad x \in [x_{S_1}], [x_{S_2}], [x_{S_3}], \tag{2}$$

$$\text{else} \quad A = 1, \quad \mathbf{u} = \mathbf{0} \quad \text{for} \quad y = 0, \tag{3}$$

$$A = 0, \quad \mathbf{u} = \mathbf{0} \quad \text{for} \quad y > 0, \tag{4}$$

where $y = 0$ denotes the top boundary of our domain where the inhomogeneous boundary conditions are introduced. The concentration of the species A is varied along the top surface, with A_S and A_F denoting the dimensional concentration of salt in the streamer and in the fingers, respectively. $[x_{S_1}], [x_{S_2}], [x_{S_3}]$ denote intervals across the top boundary where the streamers are introduced by a boundary value $A_S/A_F > 1$ (as shown at the top of Fig. 7). Use of Darcy's law in the present context should be considered as a first approximation in which some physics may be missing due to the finite—albeit small—gap of the Hele-Shaw cell used for the experiments. Another numerical model based on Brinkman's or Stokes' laws could, for instance, indicate whether or not the averaging in the wall normal direction affects the results reported below.

The numerical simulations were performed using the finite-volume code YALES2 [31–33]. The simulations were run in a domain of $32\,768 \times 16\,384$ nondimensional units with periodic boundary conditions along the horizontal direction and no flux for the concentrations along the lower boundary. The domain size considered was large enough for the dynamics not to be influenced by the lower boundary, with simulations running up to 10^5 time units. An overview of the flow dynamics is shown in Fig. 7 where the spatial distribution of the gradients of density are shown between 0 and 0.001. In the present case, the density of the streamer is considered to be four times larger than that of the finger such that $A_S/A_F = 4$. The intervals $[x_{S_1}], [x_{S_2}], [x_{S_3}]$ extend over 80 nondimensional unit lengths and are resolved by five grid points. The dynamics of the fingers and streamers were not impacted when choosing other interval sizes and grid resolutions. The instability is triggered by introducing a small perturbation for the concentration field throughout the domain, rather than only at the horizontal initial interface, as we expect the disturbances to be similar throughout an experimental setup. The unstable density difference between the fingers and the streamers with their surroundings results in a deformation of the initially growing diffusive boundary layer. Once the fingers and streamers are macroscopic they accelerate downwards with little lateral motion, such that the depth of the fingered zone remains roughly constant along the horizontal direction. With the passage of time, once the fingers are sufficiently long, they begin interacting with their neighbors, which can lead to their merging. In particular, we see that adjacent fingers are attracted by the larger streamers and merge with them after a while. Throughout this process, the gradients of density are localized along the edges of the fingers and the streamers, particularly at the lower tip.

We compute the speeds of descent of the fingers and the streamers by computing the evolution of their corresponding mixing zone. For this, we compute the extent of the downward tip of the fingers and the streamers from the horizontal interface and calculate the speed as the slope of the growth of
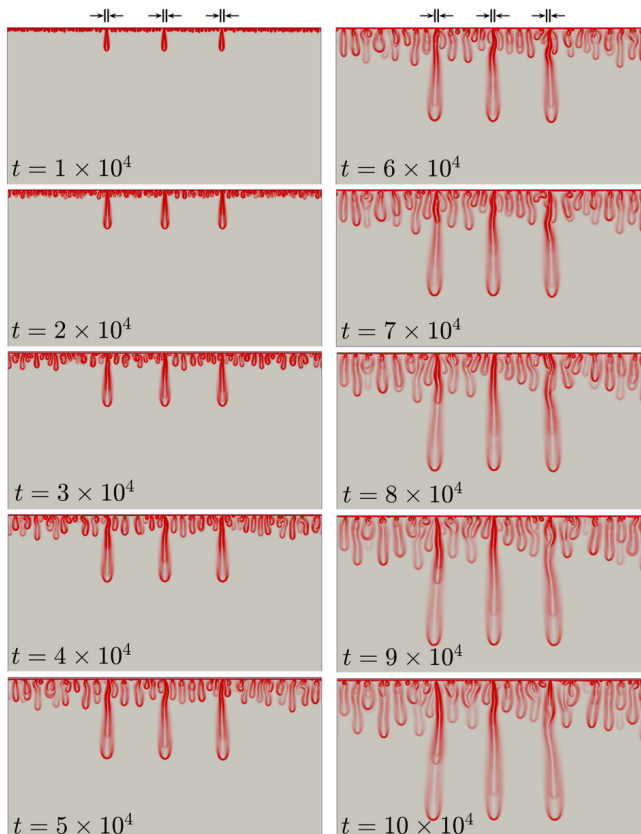
FIG. 7. Spatial distribution of the density gradients at the dimensionless times indicated in the panels.

this mixing length as a function of time. As seen earlier from the numerical snapshots, the velocities of the fingers and the streamers are influenced by the density difference when compared to their surroundings. The ratio U_S/U_F of the velocities U_S of the streamers and U_F of the fingers as a function of their corresponding concentration ratios directly proportional to their density ratios is shown in Fig. 8. Each data point shown is an average over 20 numerical simulations. A linear trend between the ratio of velocities and the ratio of densities is observed, as shown using a red line. As expected, when the density at the top of the fingers and the streamers are the same ($A_S/A_F = 1$), they evolve at the same rate leading to a velocity ratio of 1. However, if more salt is released at a given location ($A_S/A_F > 1$, an equivalent to the "real case," where brine channels would locally add more salts from draining the colder, more saline brine from the ice above), streamers with larger vertical speed develop. From Fig. 8, we can see that interactions between the fingers and streamers do not have a significant effect, and that the ratio U_S/U_F is linearly increasing with A_S/A_F. This confirms that it is appropriate to use such a linear scaling to compute below the relative mass fluxes of the fingers and the streamers.

VI. DISCUSSION

A. Evolution of the dynamics

The evolution of the experimental dynamics over time can be best seen in the space-time plots and in the videos in the Supplemental Material [23]. There is an initial time period where the critical conditions for internally driven convection are not met during which fingers are the only brine
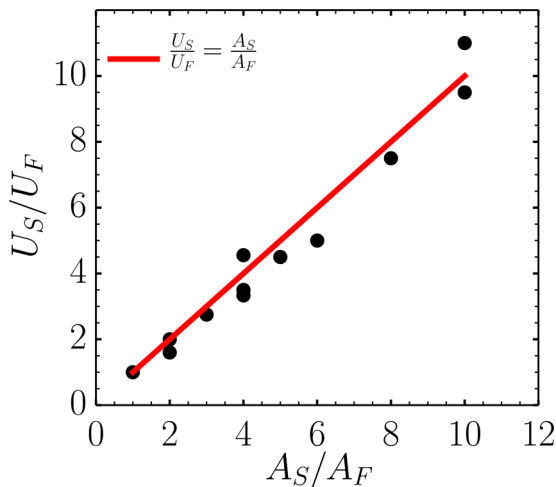
FIG. 8. Dependence of the ratio of velocities U_S of the streamer and U_F of the finger as a function of A_S/A_F. Different points for a same ratio A_S/A_F correspond to different pairs of absolute values of A_s and A_f. Each data point corresponds to an average over 20 numerical simulations. A linear scaling is observed.

rejections present. After approximately 10 mm of ice growth, internal convection starts, resulting in the appearance of additional deeper penetrating streamers emanating from brine channels in the ice. It is possible that these features are similar to those of Wettlaufer *et al.* [18] who observed that weak initial rejections interpreted as interfacial convection were replaced by stronger internally driven rejections after a certain time. The onset of internal convection in the current experiments occurs for a lower thickness of ice than in [18] and the interfacial convection seen here was not replaced by internal convection, rather the two mechanisms occur together. However, direct comparison is difficult between these experiments as the observations of the previous work were carried out in a 3D tank, whereas here the cell is closer to 2D.

Once internal convection is initiated and streamers are present, an alternation of phases of higher and lower streamer activity is reflected in the on-off behavior of individual streamers and also on a larger scale in the evolution of the mixing length [see Fig. 6(a)]. This on-off behavior has previously been observed by Eide *et al.* [34] in a salt water system and suggested to be due to the return of fresher water upwards through the channel. It has also been predicted by a simple model based on considerations of local Rayleigh numbers [35].

This intermittent behavior must be due to the evolution of processes within the brine channel structures. We hypothesize that the original salt rejection depletes the brine reservoir of the streamer, such that a period of re-establishment (replacement of channel brine by sea water from the upward "diffused" branch of the convective cell, followed by cooling and thermodynamic re-adjustment leading to increasing brine concentration in the upper part of the channel) must occur before a new channel can restart as a drainage conduit. Unfortunately, due to the limitations of the Schlieren method mentioned previously, flow within channels is not directly observed, so we are unable to determine if the off period corresponds to an upflow within the channel [19].

The evolution of the mixing length, which represents an average of several streamers [Fig. 6(a)], shows that the channels are experiencing this evolution similarly. This evolution is particularly evident when all of the streamers within the field of view stop at the same time [Figs. 4(d) and 6(a)]. Albeit similar, the evolution is not identical, as evidenced by the range of speeds (and hence densities; see Sec. V) measured for individual streamers at the same time [Fig. 6(b)]. Differences in individual streamer evolution may be related to geometric factors such as a different volume of ice drained by each channel.

The episodic on-off behavior of the streamers is in contrast to the continuous generation of fingers. The continuity of the fingers supports their formation as density-driven fingers descending from a continuously enriched boundary layer and is similar to previous observations of interfacial convection in an aqueous ammonium chloride system visualized using dye injection [36,37]. The presence of a continuous interfacial mechanism is consistent with gas fractionation data [38,39], which requires that brine is not mixed throughout the ice layer, which would be the case with a density-driven convective cycle taking place entirely through internal convection.

B. Relative density of fingers and streamers

The relative speeds of fingers and streamers, combined with the qualitative difference in refractive index, allow us to say that the fingers are less dense than the streamers. The density of the brine in either fingers or streamers is a function of their salinity and temperature. From thermodynamical considerations we are able to discount an effect of temperature on the density. Indeed, in the case of a cylindrical brine conduit of 1 mm diameter within an ice layer cooled from above, the temperature of the liquid inside the conduit equilibrates rapidly by diffusion to the surrounding ice. We can therefore consider that the temperature of the brine streamer as it exits the ice layer is the same as the temperature of the ice at that point, i.e., the same temperature as the fingers emanating from the boundary layer. We can therefore assume that any differences observed between speeds of fingers and streamers are due to a salinity difference between them, originating from different salinity enhancement mechanisms.

Brine drainage channels are a source of brine along almost the entire depth of the ice [4], so the final salinity of the streamers will be a mixture of the brine salinities possible within the ice cover. The brine concentration is controlled by the temperature of the ice (the lower the temperature, the higher the concentration). We know that the temperature of the top of an ice layer will be approximately that of the forcing temperature (here the temperature of the cooling lid, $-20\,°C$), with a linear temperature profile to the base of the ice layer [40], which will be at the freezing point of the aqueous solution ($-1.92\,°C$ for a 35 ppt NaCl solution [41]). Therefore, in an ice layer cooled from above, the higher the brine is in the ice layer, the higher its salinity.

On the other hand, the boundary layer at the ice-water interface will show a concentration dependent on the balance between the salt segregation at the freezing front, the growth rate of the ice, and the diffusion of salt from the boundary layer to the bulk water layer. As the brine here is not trapped within the ice layer and shows a temperature very close to the freezing point, it does not become as concentrated as the brine evacuated by channels.

As the growth rate of the ice decreases in time (see Fig. 3), we might expect the density (and hence the descent speed) of the fingers to also decrease, as the rate of diffusion becomes higher than the rate of progression of the ice layer. However, our observations do not show any appreciable change in the speed of fingers over the course of the experiments [Fig. 6(b)]. It is possible that the ice growth rate is still sufficiently high when compared to salt diffusion rate from the boundary layer into the bulk such that the boundary layer is enhanced to the same degree before convection begins.

C. Relative mass flux

The linear relationship between the ratio of descent speeds and the ratio of densities between the finger/streamer and the bulk (Sec. V) can be combined with the measured descent speeds to consider the relative mass flux of brine transported through streamers and fingers. To do this we calculate the "mass excess" (Δm) of a given rejection, which we define as the difference in mass m of a same volume of the rejection and of the bulk liquid. For simplicity, we will write the following equations for a streamer, but they are equally valid for a finger:

$$\Delta m_s = m_s - m_{\text{bulk}} = \rho_s V_s - \rho_b V_s = V_s \Delta \rho_s, \tag{5}$$

where m_s is the mass of a given volume V_s of a streamer, m_{bulk} is the mass of an equivalent volume of solution at the salt concentration of the bulk, ρ_s is the density inside the streamer, and ρ_b is the

density of the bulk, $\Delta\rho_s = \rho_s - \rho_b$. If we consider that V_s is the volume expelled at the brine channel exit during a time interval δt, we assume that

$$V_s = \pi R_s^2 u_s \delta t, \tag{6}$$

where u_s is the speed of descent of the streamer and R_s is the observed radius of the streamers as they descend in the underlying water layer after exiting the brine channel.

Combining Eqs. (5) and (6), we see that the excess mass Δm_s expelled by one streamer during δt becomes

$$\Delta m_s = \pi R_s^2 u_s \delta t \Delta\rho_s. \tag{7}$$

Similarly, we can write for the fingers that

$$\Delta m_f = \pi R_f^2 u_f \delta t \Delta\rho_f, \tag{8}$$

where R_f is here the average radius of the fingers resulting from the instability of the solutal boundary layer. Radii of streamers and fingers have been measured using their average width on the experimental images. Specifically, a rejection is taken in a Schlieren image as a vertical band whose refractive index differs from the background, becoming lighter or darker (as shown in Fig. 2). The diameter of the "cylindrical" rejection is therefore measured as the pixel distance between the brighter and darker side of the rejection. The average radii from this method are approximately $R_s = 0.5$ mm for a streamer and $R_f = 0.35$ mm for a finger. Both radii are thinner than the width of the cell, and, therefore, the convective zone can be assumed to be a cylinder.

The ratio of excess mass expelled by one streamer and one finger during the same period of time or equivalently, the ratio of mass fluxes becomes then

$$\frac{\Delta m_s}{\Delta m_f} = \frac{R_s^2 u_s \Delta\rho_s}{R_f^2 u_f \Delta\rho_f}. \tag{9}$$

As the number of streamers and fingers are not the same, the total mass flux for the observed width of ice must take into account this difference, so the mass flux ratio for the total number of streamers and fingers becomes

$$\frac{\Delta M_s}{\Delta M_f} = \frac{R_s^2 u_s \Delta\rho_s n_s}{R_f^2 u_f \Delta\rho_f n_f}, \tag{10}$$

where $\Delta M_s = n_s \Delta m_s$, $\Delta M_f = n_f \Delta m_f$, where n_s and n_f are the number of streamers and fingers, respectively.

Using a linear relationship between $\Delta\rho_s/\Delta\rho_f$ and u_s/u_f, and noting that $R_s^2/R_f^2 \sim 2$, we have

$$\frac{\Delta M_s}{\Delta M_f} \sim 2\left(\frac{u_s}{u_f}\right)^2 \frac{n_s}{n_f}. \tag{11}$$

The calculated values of $\Delta M_s/\Delta M_f$ from the experimental data are shown in Fig. 9.

We see that there is a large variability related to the "on-off" behavior of the streamers inducing a change of the number of streamers in time. The ratio $\Delta M_s/\Delta M_f$ is always greater than unity showing that, when streamers are present, there is more salt rejected through internal convection than through interfacial convection. Under these conditions, the flux from the streamers varies between 2 and 18 times that of the fingers. When streamers are very active (i.e., large $\Delta M_s/\Delta M_f$), then the salt rejection by fingers has a smaller relative contribution to the total flux, which can explain why their contribution is difficult to measure in the field. Note, however, that our results show that, for the "baseline" minimal mass flux ratio (dotted line in Fig. 9), nearly 30% of the salt comes from fingers. Their contribution can even represent up to 100% of the salt rejected when no streamer is active.

The contribution from fingers becomes especially nonnegligible if we consider the variability of brine rejection from brine channels. The speeds of streamers reported here are necessarily those
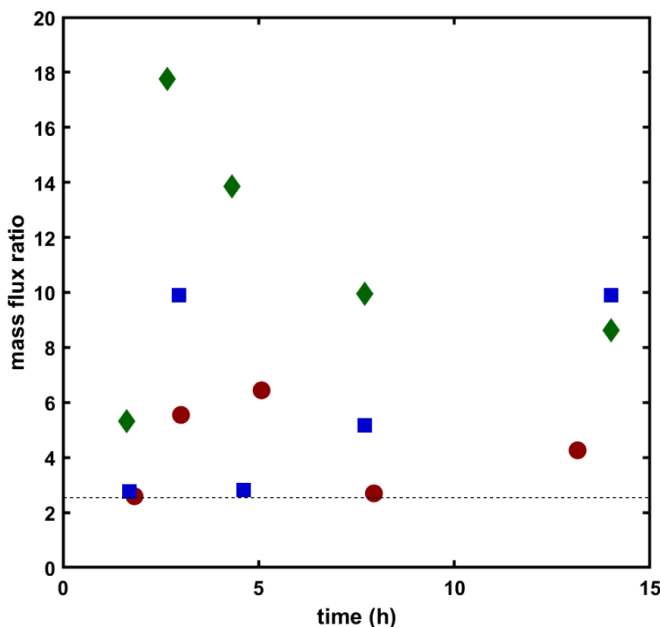
FIG. 9. Mass flux ratio $\Delta M_s / \Delta M_f$ as a function of time for the three experiments when streamers are present and descent speed is measurable.

where streamers are active. However, these streamers are not maintained constantly, particularly during periods of low to zero streamer activity, so the estimate of the mass flux from streamers is an upper bound. It is likely that the contribution of fingers to the total flux is thus larger than usually thought. Indeed, for some time intervals, when the number of streamers is low, the finger flux can be similar to that of streamers. When streamers are absent, the flux of fingers is then obviously stronger than the streamer flux.

The ratio of mass fluxes estimated here is therefore different to the observations of Notz *et al.* [15] in the field, where salt segregation was not observed. We suggest that a low-level constant expulsion of brine through interfacial convection, although not easy to detect at the resolution of the field measurements, might be more important than previously thought. The contribution of salt transport through salt segregation at the interface would thus be not negligible, at least in the initial stages of ice growth under these experimental conditions and when streamers are absent. Further studies should investigate if this state continues throughout ice growth under different conditions.

Note that a limitation of our analysis is that the temporal resolution of measurements in Fig. 9 is relatively low because of the sparse resolution of Fig. 6(b) on which it is based. Velocity measurements can be made only from the Schlieren images when streamers are observed to start (or restart) from the ice layer, as without any plume base visible in the Schlieren image, it is not possible to measure the velocity of a streamer. Therefore, we could collect data points only at times when enough streamer velocities could be measured within a suitable range of time to allow for an average velocity to be calculated. For consistency, the number of streamers [Fig. 5(a)] and data on finger number and velocities were measured at the same time as streamer velocities. Note also that because of the variability of movements of streamers and fingers, due to interactions between them, the on-off behaviors, and the fact that the interface is a moving boundary, it remains challenging to perform automated analysis of the data at higher frequencies. Schlieren imaging allows rejections of different refractive index to be visualized, without introducing foreign material to the system, which would interfere with the dynamics. However, this technique comes with the constraint that the system must be quasi-2D, as multiple rejections in the third dimension would be projected onto the same position in the Schlieren image and therefore undistinguishable. This constraint on the

dimensionality of the cell may result in effects on the dynamics, both in the growing ice layer, e.g., for brine catchment areas, and in the underlying water layer. Future work should consider these effects.

VII. CONCLUSIONS

In this study, we have carried out experiments growing an ice layer from a 35 ppt NaCl solution in a quasi-2D Hele-Shaw cell. Observations of the brine rejections from the growing ice layer were made by combining Schlieren and direct imaging systems. Two distinct brine rejection mechanisms have been characterized: numerous interfacial fingers driven by a boundary layer instability when salt is rejected from the growing ice, joined later by a smaller number of internally driven, faster, and longer descending streamers, originating from brine channels in the sea ice layer. The Schlieren visualization clearly shows that, while the long streamers exhibit an on-off behavior, short fingers are present throughout the dynamics. Numerical simulations have indicated that, despite interaction between fingers and streamers, the ratio of their downward speed still scales linearly with the ratio of their densities.

An estimation of the mass flux through interfacial and internal convection shows that, when streamers are present, they transport more mass than fingers as they are more concentrated. Nevertheless, sometimes streamers are present in a very low number or even are totally absent while the fingers remain always present in a large number. In that case, the contribution of fingers to the total salt flux might be larger than expected.

The results of these experiments show that combining Schlieren and direct imaging is a useful method for observing the processes occurring within and underneath a growing sea ice layer in a Hele-Shaw cell. These observations lead us to suggest that interfacial convection may be more important as a brine rejection mechanism than previously thought, and the importance of this mechanism should be further investigated.

ACKNOWLEDGMENTS

---

[1] M. G. Worster, Convection in mushy layers, Annu. Rev. Fluid Mech. **29**, 91 (1997).

[2] D. L. Feltham, N. Untersteiner, J. S. Wettlaufer, and M. G. Worster, Sea ice is a mushy layer, Geophys. Res. Lett. **33**, L14501 (2006).

[3] A. J. Wells, J. R. Hitchen, and J. R. G. Parkinson, Mushy-layer growth and convection, with application to sea ice, Phil. Trans. R. Soc. A **377**, 20180165 (2019).

[4] W. F. Weeks, *On Sea Ice* (University of Alaska Press, Fairbanks, 2010).

[5] W. F. Weeks and S. F. Ackley, The growth structure and properties of sea ice, in *The Geophysics of Sea Ice*, NATO ASI Series, edited by N. Untersteiner (Springer, Boston, MA, 1986), pp. 9–164.

[6] A. E. Gill, Circulation and bottom water production in the Weddell Sea, Deep Sea Res. Oceanogr. Abstr. **20**, 111 (1973).

[7] K. Aagaard, L. K. Coachman, and E. Carmack, On the halocline of the Arctic Ocean, Deep Sea Res. A **28**, 529 (1981).

[8] J. Morison, M. McPhee, R. Muench, and The LeadEx Group, The LeadEx experiment, Eos Trans. Am. Geophys. Union **74**, 393 (1993).

[9] K. I. Ohshima, Y. Fukamachi, and G. D. Williams, Antarctic bottom water production by intense sea-ice formation in the Cape Darnley polynya, Nat. Geosci **6**, 235 (2013).

[10] M. Vancoppenolle, K. M. Meiners, and C. Michel, Role of sea ice in global biogeochemical cycles: Emerging views and challenges, Quat. Sci. Rev. **79**, 207 (2013).

[11] J. Zhou, B. Delille, and H. Eicken, Physical and biogeochemical properties in landfast sea ice (Barrow, Alaska): Insights on brine and gas dynamics across seasons, J. Geophys. Res. Ocean **118**, 3172 (2013).

[12] M. Thomas, M. Vancoppenolle, J. L. France, W. T. Sturges, D. C. E. Bakker, J. Kaiser, and R. von Glasow, Tracer measurements in growing sea ice support convective gravity drainage parameterizations, J. Geophys. Res.: Oceans **125**, e2019JC015791 (2020).

[13] J. S. Wettlaufer, M. G. Worster, and H. E. Huppert, The phase evolution of young sea ice, Geophys. Res. Lett. **24**, 1251 (1997).

[14] G. F. N. Cox and W. F. Weeks, Brine drainage and initial salt entrapment in sodium chloride ice, CRREL Res. Rep. **345**, 85 (1975).

[15] D. Notz, J. S. Wettlaufer, and M. G. Worster, A non-destructive method for measuring the salinity and solid fraction of growing sea ice in situ, J. Glaciol. **51**, 159 (2005).

[16] K. M. Golden, The percolation phase transition in sea ice, Science **282**, 2238 (1998).

[17] M. G. Worster, Instabilities of the liquid and mushy regions during solidification of alloys, J. Fluid Mech. **237**, 649 (1992).

[18] J. S. Wettlaufer, M. G. Worster, and H. E. Huppert, Natural convection during solidification of an alloy from above with application to the evolution of sea ice, J. Fluid Mech. **344**, 291 (1997).

[19] C. A. Middleton, C. Thomas, A. De Wit, and J.-L. Tison, Visualizing brine channel development and convective processes during artificial sea-ice growth using Schlieren optical methods, J. Glaciol. **62**, 1 (2016).

[20] C. A. Middleton, C. Thomas, J.-L. Tison, D. M. Escala, and A. De Wit, Imaging the evolution of brine transport in experimentally grown quasi-two-dimensional sea ice, Procedia IUTAM **15**, 95 (2015).

[21] M. Wakatsuchi and N. Ono, Measurements of salinity and volume of brine excluded from growing sea ice, J. Geophys. Res. **88**, 2943 (1983).

[22] G. S. Settles, *Schlieren and Shadowgraph Techniques* (Springer, Berlin, 2001).

[23] See Supplemental Material at http://link.aps.org/supplemental/10.1103/PhysRevFluids.7.043503 for a time-lapse video of Schlieren (left) and direct (right) visualisation of brine transport pathways during ice growth from a salt water solution in a quasi-2D Hele-Shaw cell.

[24] E. Guyon, J.-P. Hulin, L. Petit, and C. Mitescu, *Physical Hydrodynamics* (Oxford University Press, Oxford, 2001).

[25] T. P. Schulze and M. G. Worster, A numerical investigation of steady convection in mushy layers during the directional solidification of binary alloys, J. Fluid Mech. **356**, 199 (1998).

[26] R. F. Katz and M. G. Worster, Simulation of directional solidification, thermochemical convection, and chimney formation in a Hele-Shaw cell, J. Comput. Phys. **227**, 9823 (2008).

[27] A. J. Wells, J. S. Wettlaufer, and S. A. Orszag, Maximal Potential Energy Transport: A Variational Principle for Solidification Problems, Phys. Rev. Lett. **105**, 254502 (2010).

[28] A. C. Slim, M. M. Bandi, J. C. Miller, and L. Mahadevan, Dissolution-driven convection in a Hele-Shaw cell, Phys. Fluids **25**, 024101 (2013).

[29] C. Thomas, S. Dehaeck, and A. De Wit, Convective dissolution of CO_2 in water and salt solutions, Int. J. Greenhouse Gas Control **72**, 105 (2018).

[30] A. De Wit, Chemo-hydrodynamic patterns and instabilities, Annu. Rev. Fluid Mech. **52**, 531 (2020).

[31] S. S. Gopalakrishnan, J. Carballido-Landeira, A. De Wit, and B. Knaepen, Relative role of convective and diffusive mixing in the miscible Rayleigh-Taylor instability in porous media, Phys. Rev. Fluids **2**, 012501(R) (2017).

[32] V. Moureau, P. Domingo, and L. Vervisch, Design of a massively parallel CFD code for complex geometries, C. R. Mécanique **339**, 141 (2011).

[33] S. S. Gopalakrishnan, J. Carballido-Landeira, B. Knaepen, and A. De Wit, Control of Rayleigh–Taylor instability onset time and convective velocity by differential diffusion effects, Phys. Rev. E **98**, 011101(R) (2018).

[34] L. I. Eide and S. Martin, The formation of brine drainage features in young sea ice, J. Glaciol. **14**, 137 (1975).

[35] D. W. Rees Jones and M. G. Worster, A physically based parameterization of gravity drainage for sea-ice modeling, J. Geophys. Res.: Oceans **119**, 5599 (2014).

[36] C. F. Chen, Experimental study of convection in a mushy layer during directional solidification, J. Fluid Mech. **293**, 81 (1995).

[37] C. F. Chen and F. Chen, Experimental study of directional solidification of aqueous ammonium chloride solution, J. Fluid Mech. **227**, 567 (1991).

[38] J.-L. Tison, C. Haas, and M. M. Gowing, Tank study of physico-chemical controls on gas content and composition during growth of young sea ice, J. Glaciol. **48**, 177 (2002).

[39] F. Brabant, Physical and biogeochemical controls on the DMS/P/O cycles in Antarctic sea ice, Ph.D. thesis, Université libre de Bruxelles, 2012.

[40] C. Petrich and H. Eicken, Overview of sea ice growth and properties, in *Sea Ice*, 3rd ed., edited by D. N. Thomas (John Wiley and Sons, 2017), p. 667.

[41] F. J. Millero, Freezing point of seawater. Annex 6, Eight report of the Joint Panel on Oceanographic Tables and Standards (JPOTS). UNESCO technical papers in marine sciences, **28**, 29 (1978).